FLUID FLOW AND HEAT TRANSFER ANALYSIS OF THE VHTR LOWER PLENUM USING THE FUEGO CFD CODE

Sal B. Rodriguez[1,3], Stefan Domino[2], and Mohamed S. El-Genk[3]

[1]Sandia National Laboratories, P.O. Box 5800, MS 0748, Albuquerque, NM 87185-0748, sbrodri@sandia.gov, (505) 284-2808
[2]Sandia National Laboratories, P.O. Box 5800, MS 0836, Albuquerque, NM 87185-0836, spdomin@sandia.gov, (505) 284-4317
[3]Chemical and Nuclear Engineering Dept. and Institute for Space and Nuclear Power Studies University of New Mexico, Albuquerque, NM 87131, mgenk@unm.edu, (505) 277-5442

Abstract
There are a number of safety and heat transfer issues in the lower plenum (LP) of a prismatic core very high temperature reactor (VHTR), such as the formation of hot spots in the lower support plate and thermal stratification of the helium gas coolant. In this paper, results of key separate-effect validation and verification (V&V) calculations, as well as the calculated flow fields and heat transfer characteristics in the LP are presented and discussed. The calculations with helium gas at 1,273 K were performed with Fuego, a 3D, massively parallel, unstructured element, computational fluid dynamics (CFD) code being developed at Sandia National Laboratories. The calculations employed the dynamic Smagorinsky large eddy simulation (LES) turbulence model, participating media radiation (PMR), and 1D conjugate heat transfer (CHT). The results qualified the impact of using swirling helium gas flow into the LP to minimize the effect of the hot spots and enhance heat transfer in the bottom plate and mixing in the LP.

[1]Sandia is a multiprogram laboratory operated by Sandia Corporation, a Lockheed Martin Company, for the United States Department of Energy's National Nuclear Security Administration under Contract DE-AC04-94AL85000.

1. INTRODUCTION

One of the original goals of the very high temperature reactor (VHTR) is the generation of hydrogen, which will require operating at temperatures ranging from 1,000 – 1,273 K (MacDonald *et al*., 2003; Southworth, 2004; Schultz *et al*., 2004; MacDonald, 2004; INL, 2007). The helium gas coolant in the reactor core region flows at very high velocity, up to 70 m/s, to remove the heat generated by fission in the coated fuel particles dispersed in graphite. The combination of high exit temperature and flow velocity of the helium coolant into the lower plenum (LP) of a VHTR contributes a number of safety and heat transfer issues requiring detailed assessment and investigation. Particular issues of interest are the formation of hot spots in the lower support plate and the thermal stratification of the helium gas coolant. Hot spot formation is caused by impingement onto the LP walls by helium jets that are as much as 200 K hotter than average. On the other hand, the thermal stratification in the LP results from poor mixing of helium within the LP cavity. The flow field in the LP region is quite complex, caused by interacting jet flows from the numerous helium coolant channels and the presence of a large number of graphite support posts. As a result, the LP is expected to have cross flows, flow stagnation zones, vortex interaction, vortex shedding, entrainment, large variation in Reynolds number (Re), recirculation, and mixing enhancement and suppression regions.

Computational fluid dynamics (CFD) have been used successfully to investigate the above two operation and safety issues in the LP, and have also aided in the development of viable means to mitigate the impact of the hot spots and thermal stratification (Guililen and McIlroy, 2007; McIlroy, McEligot, and Pink, 2008; Johnson, 2009a, 2009b; Johnson and Schultz, 2009; Rodriguez and El-Genk, 2010a). This research

investigates swirl inserts at the exit of the helium gas flow channels in the VHTR core to minimize the formation of hot spots and enhance mixing of the helium gas coolant. The investigations are carried out using the Sandia National Laboratories' (SNL) Fuego CFD code, and included the dynamic Smagorinsky large eddy simulation (LES) turbulence model, participating media radiation (PMR), and 1D conjugate heat transfer (CHT). The calculation results are validated using reported experimental results of key phenomena expected to occur in the VHTR LP. The computational models, the validation and verification (V&V) calculations, and the obtained results are presented and discussed in the following sections.

2. KEY FUEGO CFD MODELS

Fuego is one of a set of strategic, comprehensive codes currently being developed through the Advanced Simulation and Computing (ASC) program at SNL. Fuego is a low Mach number, reactive flow, generalized unstructured code that includes laminar, buoyant, and turbulent flow models, flux limiters, combustion, PMR, and CHT. Through user input, Fuego can also be coupled to heat conduction and enclosure radiation models, as well as other ASC tools for additional physics calculations. Simulation capabilities in Fuego include the state-of-the-art turbulence models for Reynolds-averaged Navier-Stokes (RANS) and LES. The RANS models include v2-f, low Re k-ε, standard k-ε, k-ω, time filtered Navier-Stokes (TFNS), as well as many others. Among Fuego's more sophisticated LES models are the KSGS, Smagorinsky, and dynamic Smagorinsky models. For the 3D anisotropic turbulent flow fields and complex mixing expected in the LP of the VHTR during nominal operation, the v2-f, Smagorinsky, dynamic Smagorinsky, and TFNS models are most appropriate and could be more accurate than other options. Fuego also includes Lagrangian transport capabilities appropriate for modeling particles and drops, some deposition modeling physics, and basic chemistry models.

2.1 Turbulence Modeling

Turbulent flow encountered in the VHTR LP involves wide ranges of length and time scales, requiring massive computational resources to directly resolve the physical processes for even simplified high-Re problems. Modeling approximations must be made to solve complex problems of interest within a reasonable amount of computational time. Two types of turbulence modeling are commonly employed in engineering processes and applications, namely; (a) the RANS method in which the time-averaged equations are solved, and (b) LES, which relies on spatial filtering.

In the RANS modeling approach, an isotropic turbulence viscosity is introduced to provide closure for the Reynolds stress terms. This involves the modified Boussinesq turbulent viscosity approximation. The stress closure can be handled by a variety of modeling techniques. For example, for the k-ω model (Wilcox, 1998), the turbulence viscosity is expressed by the relationship:

$$\mu_t = \rho \frac{k}{\omega}. \qquad (1)$$

In the above equation, ρ is the fluid density, k is the turbulent kinetic energy, while ω is the specific dissipation rate. Details of the k-ω model are presented elsewhere (Wilcox, 1998).

In the present calculations, we employed the LES method with the dynamic Smagorinsky closure model (Germano *et al*., 1991). In this method, the turbulent viscosity is expressed by the following relationship:

$$\mu_t = C_D \rho \Delta^2 |S|. \qquad (2)$$

The coefficient C_D is given by a dynamic filtering process based on the local turbulence field, Δ is the spatial filter length, and $|S|$ represents the filtered strain rate tensor magnitude. A generalized subgrid scale methodology for variable density flow is discussed in the literature (Moin, 1991).

2.2 Participating Media Radiation (PMR)

The spatial variation of the radiative intensity corresponding to a given direction and at a given wavelength within a radiatively participating material, I(s), is governed by the Boltzmann transport equation. In general, the Boltzmann equation represents a point balance between absorption, emission,

out-scattering, and in-scattering of radiation. For most engineering applications, however, the steady form of the Boltzmann equation is appropriate since the transient term only becomes important on nanosecond time scales, which are orders of magnitude shorter than the fastest chemical reaction. Under the assumptions of a non-scattering, gray media, with the turbulent fluctuation effects ignored, the Boltzmann equation for the l[th] ordinate direction is given by:

$$s_i^l \frac{\partial}{\partial x_i} I^l(s) + \mu_a I^l(s) = \mu_a \frac{\sigma T^4}{\pi}, \tag{3}$$

where s_i^l is the l[th] ordinate direction, μ_a is the absorption coefficient, and I^l is the intensity along the l[th] ordinate direction. Note that as a first-order approximation, the turbulent fluctuations for non-reacting flow are not included in the Boltzmann equation, as their impact on radiation is small compared to those of the terms that were retained. On the other hand, the turbulent fluctuations are appropriately addressed in the gas phase transport equations. When chemistry is active, the subgrid fluctuations in the radiative source term and mean absorption coefficient are included based on a presumed probability density function approach (correlations between absorption and intensity are always neglected). As noted, scattering effects are also ignored, although an isotropic scattering code capability can be activated, as warranted.

The radiation intensity boundary condition, assuming a diffuse surface, is given by:

$$I(s) = \frac{1}{\pi}\left[\tau\sigma T_\infty^4 + \varepsilon\sigma T_w^4 + (1-\varepsilon-\tau) q_j^{inc} n_j\right]. \tag{4}$$

In this expression, τ is the transmissivity, ε is the emissivity, T_∞ is the environmental temperature, and T_w is the wall temperature. Note that Kirchhoff's law employed in the above equation is used to relate emissivity, transmissivity, and reflectivity, ρ as:

$$\rho + \tau + \varepsilon = 1. \tag{5}$$

This assumes that absorptivity equals the emissivity. A quadrature set is provided to assemble the individual intensity and solve for quantities such as the scalar flux:

$$G = \sum_L w_L I^L, \tag{6}$$

and the radiative flux:

$$q_j^r = \sum_L w_L I^L s^L. \tag{7}$$

The SIERRA mechanics module responsible for the solution of the radiative transport equation is Syrinx. The underlying discretization employs a streamwise upwind Petrov-Galerkin finite element method discretization for the method of discrete ordinates (Burns, 1997). The degree of local stabilization is controlled by a comparison between the cell size and optical thickness. When the optical thickness increases, the full operator is used, while in thin regions, the Fuego code reverts to an up-winded operator. The coupling between the fluids and PMR regions is accomplished through the flux divergence source term:

$$\frac{\partial q_i^r}{\partial x_i} = \mu_a\left(4\sigma T^4 - G\right). \tag{8}$$

This source term is linearized via a Taylor series to provide a left-hand-side matrix contribution to the static enthalpy degree of freedom equation. The coupling between the PMR and fluids region is provided through the absorption coefficient and the emissive power.

2.3 1D Conjugate Heat Transfer (CHT)

A CHT problem is one in which the conductive heat transfer in a solid region is coupled to the convective heat transfer in a neighboring fluid flow. In its most general form, the coupling at the boundary between these two regions is governed by the continuity of the heat flux at the interface, as:

$$q_j^F n_j = q_j^S n_j. \tag{9}$$

In this equation, q_j^F and q_j^S are the heat flux in the fluid and solid, respectively, and the normal n_j is directed into the solid and out of the fluid.

In the generalized CHT coupling, a fluids mechanics region solving for the static enthalpy is coupled at the surface to a heat conduction equation solving for temperature (Domino *et al.*, 2007). In general, the solid heat flux can also include the effect of radiation via an augmented flux that is due to the irradiation onto or out of the surface. Oftentimes, however, a full CHT coupling is not required. Instead, a 1D approximation can be made in which an overall heat balance at the interface is performed, such as:

$$q_{in}^r + q_{in}^c = q_{out}^r + q_{out}^c . \quad (10)$$

Therefore, in this equation, the radiation and fluid solvers provide the incoming energy fluxes while the user specifies surface properties, backside heat transfer coefficients, the backside reference temperatures, and the wall thickness. The above equation is solved via Newton's method, and the resulting temperature is applied for the fluid and radiation boundary condition.

3. VALIDATION AND VERIFICATION (V&V)

Because of the high cost of building an integral, full-scale high-temperature, helium-cooled experimental facility that faithfully models the complex geometry and velocity field in the LP of a prismatic core VHTR, there is currently no such experimental data available for benchmarking the CFD calculations. Nevertheless, numerous experimental data exist for key, separate-effects phenomena that are expected to occur within the LP, as shown in Fig. 1. Therefore, our approach was to exercise Fuego through a set of key stand-alone simulations for V&V, with each simulation corresponding to a key flow phenomenon.

As noted in Sections 3.1 and 3.2, Fuego reproduced the single-effects experimental data adequately, providing confidence in the results of the full-effect LP simulations presented later in this paper.

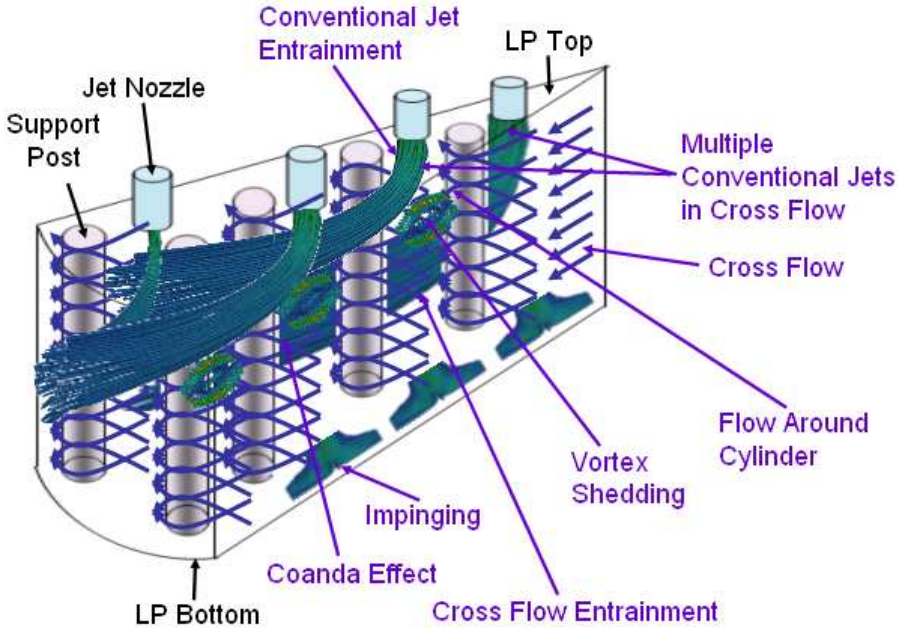

Fig. 1. Key Flow Regimes in the LP of a Prismatic Core VHTR with Conventional Jets.

3.1. Recent Fuego V&V Efforts Related to Key LP Phenomena of a VHTR

Fuego has recently undergone V&V studies for key flow phenomena in the LP of a typical VHTR that include (Rodriguez and El-Genk, 2010a, b):

1) Conventional gas jet (axial and radial velocity distribution, jet spread angle),
2) Swirling gas jet (axial and azimuthal velocity distribution),
3) Conventional gas jet in cross flow (propagation, velocity, production of counter-rotating vortices, jet cross-section),

4) Swirling gas jet in cross flow (propagation, velocity), and
5) Central recirculation zone (CRZ) formation in the flow field of swirling jets.

More recently, we simulated helium flow around a cylinder at the gas temperature properties and initial conditions expected to occur in the LP of a VHTR during nominal operation with Re ranging from 2,000 to 20,000. The calculations are discussed in Section 3.2. In general, Fuego was able to compute the key variables to within < 10% of the experimental data and/or the theoretical analytical values. The key V&V cases performed with Fuego are summarized in Table 1 below.

Table 1. Recent Fuego Validation and Verification for Key Phenomena Relevant in the LP.

Flow Type	**Key Variables/Phenomena**	**Data/Theory**	**Fuego V&V**
Conventional Jet	Axial velocity distribution	Chevray and Tutu, 1978; Schlichting, 1979; Bird, Stewart, and Lightfoot, 2007	Rodriguez and El-Genk, 2010a
	Radial velocity distribution	Reichard, 1942; Bird, Stewart, and Lightfoot, 2007	Rodriguez and El-Genk, 2010a
	Jet spread angle	Bird, Stewart, and Lightfoot, 2007; Blevins, 1992	Rodriguez and El-Genk, 2010a
Swirling Jet	Axial velocity	Blevins, 1992; Chigier and Chervinsky, 1967	Rodriguez and El-Genk, 2010a
	Azimuthal velocity	Mathur and MacCallum, 1967; Chigier and Chervinsky 1967; Billant *et al*. 1998; Blevins, 1992	Rodriguez and El-Genk, 2010a
Conventional Jet in Cross Flow	Jet propagation	Pratte and Baines, 1967; Blevins, 1992	Rodriguez and El-Genk, 2010a
	Jet velocity	Pratte and Baines, 1967; Blevins, 1992; Lim, New, and Luo, 2001	Rodriguez and El-Genk, 2010a
	Production of counter-rotating vortices	Pratte and Baines, 1967; Blevins, 1992	Rodriguez and El-Genk, 2010a
	Jet cross section (kidney)	Blevins, 1992	Rodriguez and El-Genk, 2010a
Swirling Jet in Cross Flow	Jet propagation	Kavsaoglu and Schetz, 1989; Kamotani and Greber, 1974; Denev, Frohlich, and Bockhorn, 2009	Rodriguez and El-Genk, 2010a
	Jet velocity	Kavsaoglu and Schetz, 1989; Kamotani and Greber, 1974; Denev, Frohlich, and Bockhorn, 2009	Rodriguez and El-Genk, 2010a
Flow Around a Cylinder	Stagnation pressure	White, 1991	Present study
	Vortex shedding frequency	Ribner and Etkin, 1958; Roshko, 1961; Williamson, 1989; Williamson, 1989	Present study
CRZ	Swirl angle at which CRZ is first formed.	Mathur and MacCallum, 1967; Chigier and Chervinsky, 1967; Billant *et al.*, 1998; Rodriguez and El-Genk, 2010b	Rodriguez and El-Genk, 2010b

3.2 Flow Around a Vertical Cylinder

The VHTR LP contains a large number of cylindrical graphite support posts that are approximately 8” in diameter. Due to their proximity to each other (as defined by the pitch to diameter ratio), the LP flow field is actually more similar to that around a large set of staggered tubes than to flow around a single

tube. For staggered tubes, the flow around the individual tubes interferes with the flow field, whereby the flow near the tubes never attains the approach velocity.

Flow around a vertical cylinder has been researched extensively, yielding a large experimental database and CFD simulation results (Ribner and Etkin, 1958; Williamson, 1989; White, 1991; Tutar and Holdo, 2001). In light of the simplicity of modeling the flow around a single tube and the ability to compare CFD results to well-known theory, we added the single cylinder flow calculation to our set of key Fuego V&V calculations. In the future, as warranted, we could also extend our calculations to model staggered cylinder flow. In the meantime, it could be argued that if a CFD code cannot adequately simulate the simplified flow field around a single cylinder, it most likely cannot successfully model the flow for staggered cylinders applicable to the VHTR LP.

A set of coarse and very fine rectangular meshes were generated for simulating the flow around a vertical cylinder. The meshes consisted of 4,000, 16,000, 64,000, 256,000, and 1 million hexahedral elements, which resulted in an average cell length of $2.3\text{x}10^{-2}$, $1.2\text{x}10^{-2}$, $5.7\text{x}10^{-3}$, $2.9\text{x}10^{-3}$, and $1.4\text{x}10^{-3}$ m, respectively. We noted that the solution was sufficiently converged spatially by 64,000 elements, as Fuego and theory differed by <2%. The cylinder diameter (D) was 0.203 m, the expected diameter of the graphite support posts in the LP of a VHTR. The mesh dimensions were L = 15D and W = 10D. The mesh thickness was one element. The boundaries on the x-z planes were open, and so was the boundary on the opposite end of the inflow boundary; see Fig. 2. The x-y planes had symmetry boundary conditions. The cylinder was placed 5D away from the constant velocity inflow boundary. The mesh dimensions were chosen primarily to avoid far field effects from interfering with the wake around the cylinder, and secondarily to calculate a reasonably-sized vortex street. (Note that in the actual LP, the cylinders would be much closer to each other.) Our mesh dimensions were consistent with an LES calculation found in the literature (Tutar and Holdo, 2001). The Courant-Friedrichs-Lewy (CFL) number was fixed at 1.0, which resulted in time steps of $2.7\text{x}10^{-4}$, $1.4\text{x}10^{-4}$, $4.5\text{x}10^{-5}$, $2.7\text{x}10^{-5}$, and $1.4\text{x}10^{-5}$ s, respectively. The calculations were run with eight to 256 processors on the SNL Red Sky cluster.

The calculations used helium gas at 1,273 K, which yielded a gas density of 0.0386 kg/m^3, and a kinematic viscosity of $1.36\text{x}10^{-3}$ m^2/s. The helium gas approach velocity (inflow boundary) for the calculations was fixed at 13.4, 67.0, and 134 m/s, which yielded Re of 2,000, 10,000, and 20,000. No calculations with variation in temperature were conducted for these set of calculations. However, temperature directly affects the kinematic viscosity, which affects Re, and for such reason and others, our calculations considered a 10-fold range in Re.

The problem can be better understood by using the Strouhal number (St), defined as:

$$\text{St} = \frac{f\text{D}}{\text{U}_\infty}, \tag{11}$$

where D is the cylinder diameter, f is the vortex shedding frequency, and U_∞ is the approach velocity. Figure 2 shows the vortices generated as the flow swept around the cylinder, which is known as vortex shedding (White, 1991). For a long cylinder, St can be approximated as (Wikipedia, 2010)

$$\text{St} = \text{A}\left(1 - \frac{\text{B}}{\text{Re}}\right), \tag{12}$$

for $250 < \text{Re} < 2\text{x}10^5$, which covers the regime from transition turbulence to the subcritical regime. The Wikipedia article suggests A = 0.198 and B = 19.7. However, a better data fit for the data of Ribner and Etkin (Ribner and Etkin, 1958) was found by setting A = 0.21 for $250 \le \text{Re} \le 20{,}000$, while B remained unchanged, as shown in Fig. 3. It is noteworthy that this fit also covers the low Re laminar region quite well, which is approximated by Williamson as (Williamson, 1989)

$$\text{St} = \frac{\text{A}}{\text{Re}} + \text{B} + \text{CRe}, \tag{13}$$

where A=-5.1064, B=0.2175, and C=0. Note that the streamline that is normal to the cylinder eventually impacts the cylinder wall, and because the wall is rigid, the fluid velocity is zero. The impact point is called the stagnation point (White, 1991),

$$P_S - P_\infty = \frac{1}{2}\rho U_\infty^2, \qquad (14)$$

where P_S and P_∞ are the stagnation pressure and pressure far away from the cylinder, respectively. The fluid density is ρ.

Because the pressure fluctuates with time, we employed a Reynolds average with a 0.5 s time filter. The calculated (P_S - P_∞) are shown in Table 2, while the computed St vs. Re are shown in Fig. 3. It is noteworthy that the Fuego results and theory pressure were within 0.1%, while the Fuego vortex shedding frequency was within 5% of the experimental data.

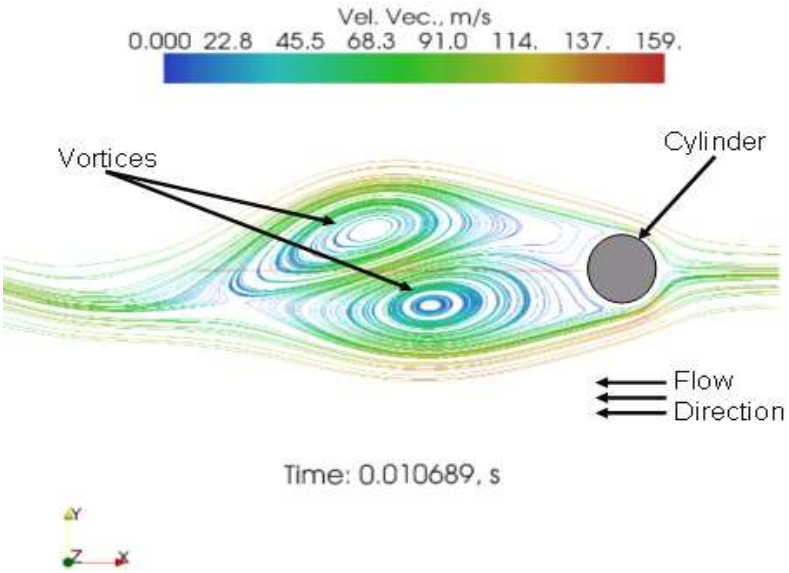

Fig. 2. Vortices Generated by Flow Around a Cylinder.

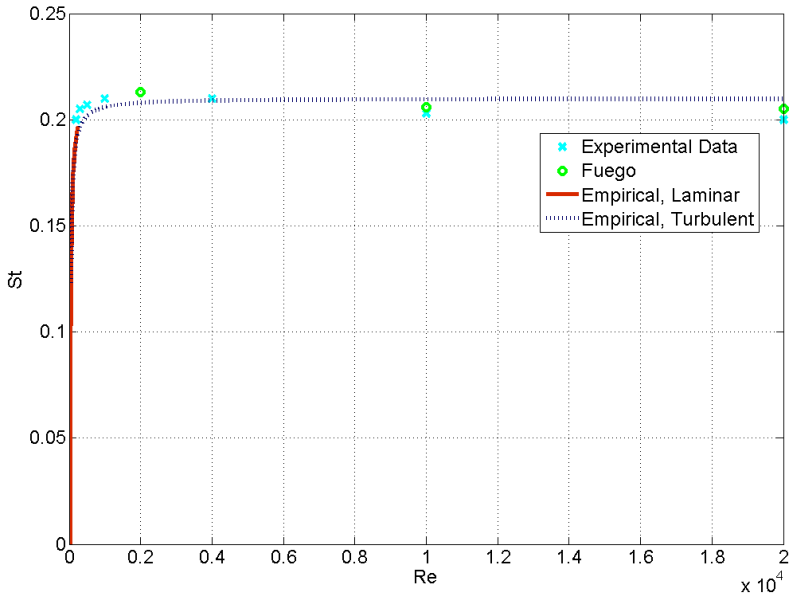

Fig. 3. Strouhal Number vs. Reynolds Number.

Table 2. Fuego $P_S - P_\infty$.

Number of Elements	$P_S - P_\infty$, Pa (Theory=86.6)
4,000	81.2
16,000	83.5
64,000	85.3
256,000	86.1
1,000,000	86.5

4. LP MODEL

Our full-scale, half-symmetry mesh of the VHTR LP consisted of 11 million unstructured hexahedral elements, which provided satisfactory spatial discretization. The model included the support posts, the helium flow channel jets, the exit, and the exterior walls, as shown in Fig. 4. Because the jets can be modeled as either conventional or swirling jet boundary conditions (BCs), the swirl number (S) can easily be changed to the desired magnitude in order to observe its impact on heat transfer and gas mixing in the LP. For the calculations employed here, we used the geometric S for a hubless swirler, which is defined as (Kerr and Fraser, 1965; Mathur and MacCallum, 1967; Bilen *et al*. 2002; Arzutug and Yapici, 2009)

$$S = \frac{2}{3}\tan(\theta). \tag{15}$$

The swirl angle is defined as the descent angle θ of the helicoid surfaces; for a conventional jet, S = 0. S is described schematically in Fig. 5.

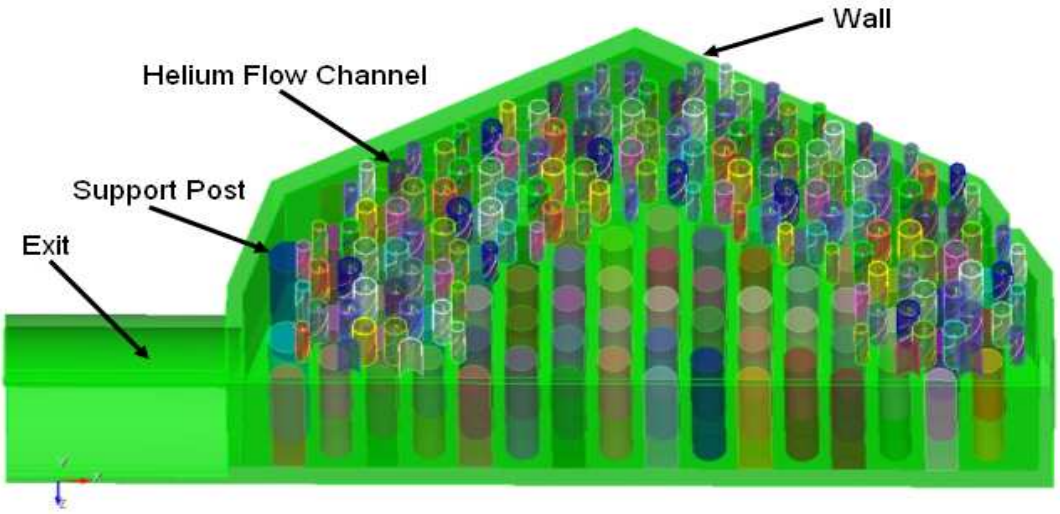

Fig. 4. Half-Symmetry Model of the VHTR LP.

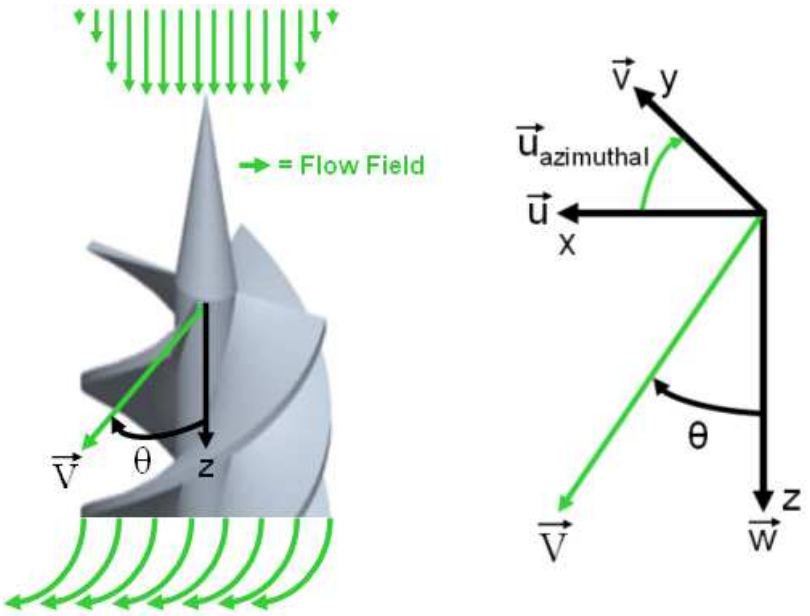

Fig. 5. Description of S and Related Flow Field.

The LP model used in the present simulations employed the dynamic Smagorinsky LES turbulence model, and included PMR and CHT. The PMR model calculated the impact of radiation heat transfer for the high temperature helium gas behavior as a participating media. For the CHT, we assumed that the LP wall conducted heat, which was subsequently convected to the ambient as a result of natural convection. The calculation mesh was generated using the CUBIT code (CUBIT, 2009) from the geometry developed with Pro/ENGINEER (PRO, 2009). The temperature-dependent physical and thermal properties for the helium were calculated using a CANTERA XML input file that was based on the Chapman-Enskog formulation (Bird, Steward, and Lightfoot, 2007).

The initial time step used was 0.01 μs, and the simulation transient time varied from 100 ms to several seconds. The time step was calculated by setting the maximum CFL to 1.0, resulting in a time step of 1.2×10^{-5} s. Three helium jets were set to 1,473 K in order to investigate their tendency to form hot spots and thermally-stratified regions; the rest of the jets were at 1,273 K. S was set to 0.67. All calculations were run on the massively parallel Thunderbird machine at SNL.

The results of the calculation are shown in Figs. 6 and 7. Figure 6 shows the calculated velocity streamlines, which have been colored with the gas temperature. The figure shows how rapidly the swirling flow jets mixed; by the time the jets had travelled approximately 60% of the distance to the bottom plate, the peak helium temperature had dropped 100 K, and by the time the jets impinged the bottom plate, the gas temperature had reached that of the surrounding, cooler gas (1,273 K). By comparison, setting S = 0 (i.e., conventional jets) with the same BCs resulted in the jet impinging on the bottom plate at ~1,325 K (Rodriguez and El-Genk, 2010c). This is a good performance metric of the entrainment and mixing capacity of the swirling jets when compared with conventional jets. Figure 7 shows the temperature contours for the three hot channels. The figure shows that the hot gas quickly reached the colder, surrounding gas temperature within about seven jet diameters. (Note: the holes in the figure are the support post locations.)

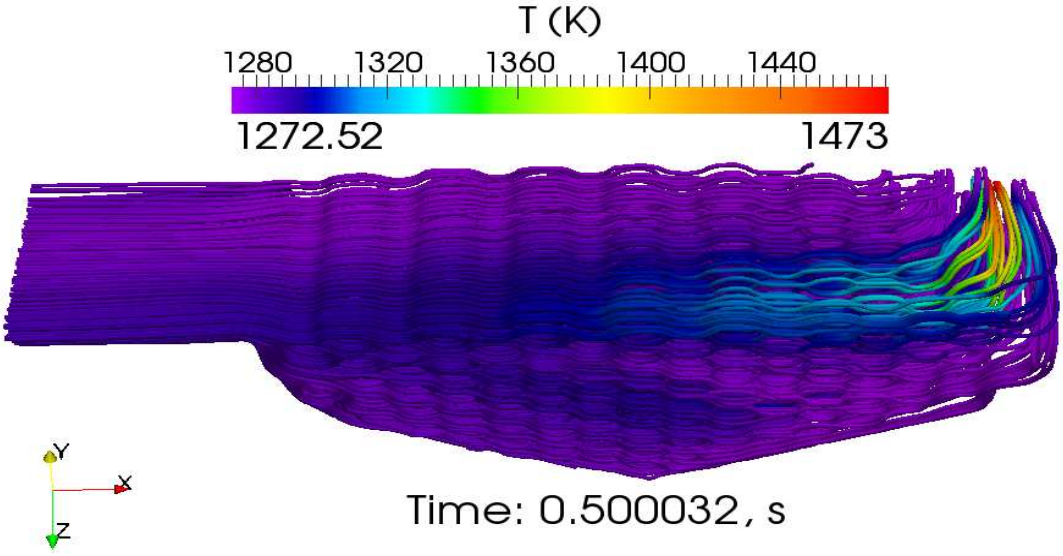

Fig. 6. Temperature Distribution Superimposed on the Velocity Streamlines.

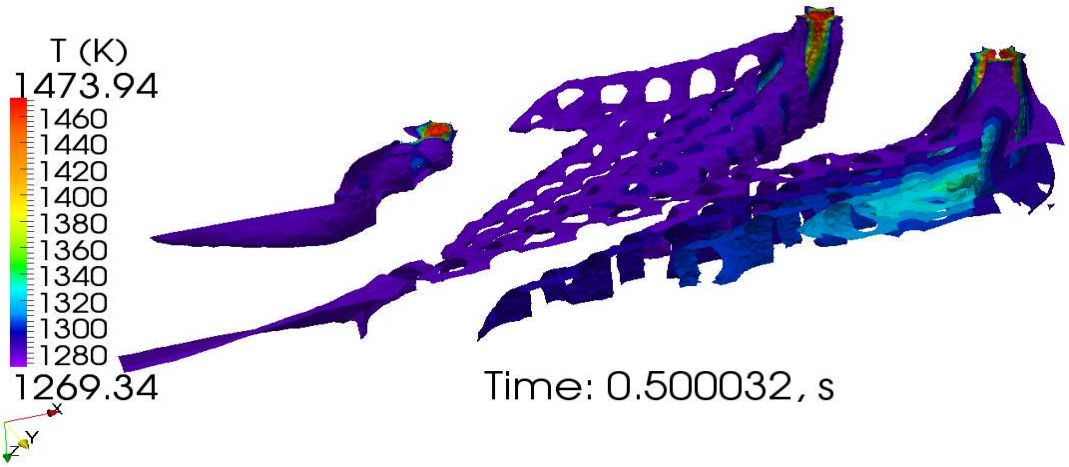

Fig. 7. Temperature Contours for the Three Hot Channels.

Finally, in order to further gauge the effect of S on cooling the bottom plate in the LP, the hexahedral element cell-averaged temperatures of a planar slice at the bottom plate (the opposite end of the jet exits) were calculated and grouped according to a linear distribution with 40 temperature "bins". To this effect, we ran a set of additional calculations with S = 0.38, 1.15, and 2.49 (i.e., θ = 30, 60, and 75º, respectively). Then, the net difference between the number of elements for all the temperature bins for each case i where S>0 and basecase S=0 were computed, i.e., $n(T_{bin,S>0})_i - n(T_{bin,S=0})$, and plotted, as shown in Fig. 8. For example, the solid blue line with circles shows the net difference in elements for each of the 40 temperature bins for the calculations with S=2.49 and S=0, and so forth. The figure shows that as S increased, the number of finite elements in the bottom plate with cooler temperature increased dramatically. For example, the case with S=2.49 had 2,573 more elements at 1,273.5 K than when S=0; the next case, S=1.15, had 889 more, while the cases for S=0.38 and 0.67 each had about 340 more such elements. Given that the planar slice consisted of 3,602 elements, the number of cooler elements as a result of the enhanced swirl field was quite significant. (Note: negative temperature-bin count in Fig. 8 means that there were more of a given bin element for the case S=0 than for S>0.) The results are reasonable, as the literature shows that the entrainment, as defined by the entrainment constant K_e, increases linearly as S increases (Kerr and Fraser, 1965):

$$K_e = 0.35 + 1.4S \quad (16)$$

and (Chigier and Chervinsky, 1967):

$$K_e = 0.32 + 0.8S\,. \quad (17)$$

Consequently, by the time S=2.49, all the finite elements in the temperature slice were only within 1 - 2 K of the surrounding, cooler helium jets (~1,270 K) vs. ~1,325 K for the basecase.

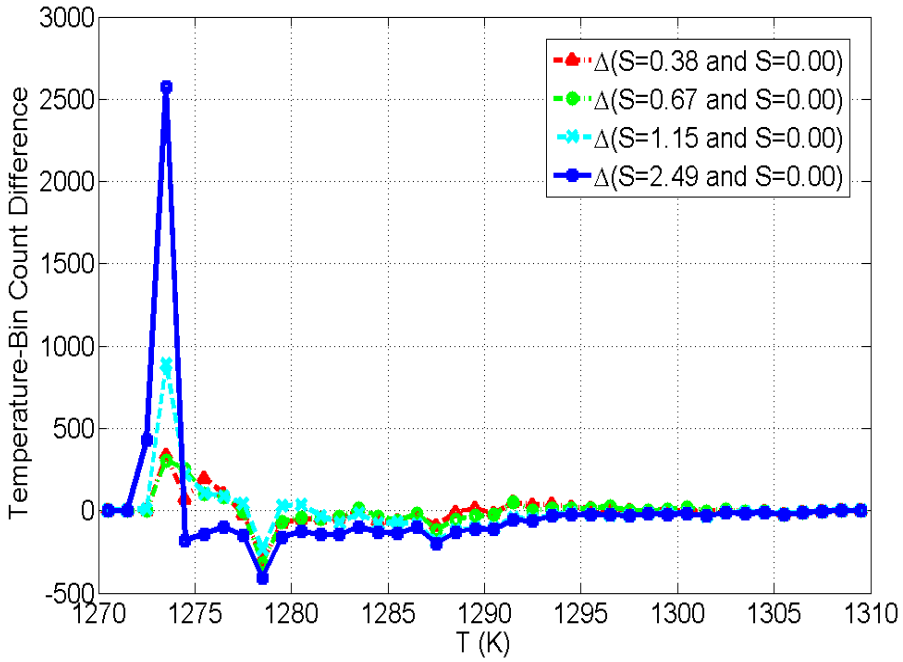

Fig. 8. Effect of S on Heat Transfer Enhancement at the Bottom Plate of the LP.

V. CONCLUSION

To establish confidence in the results of the Fuego CFD code, we simulated a set of key, separate-effects flow phenomena expected to occur in the LP of a prismatic core VHTR. The V&V calculations used helium gas at 1,273 K. The results of the V&V effort showed that Fuego predictions were generally within 10% of the reported experimental results and/or the theoretical analytical values.

We proceeded to investigate the complex flow field occurring in the LP of a typical VHTR with a prismatic core. The combination of high helium gas velocity and high temperature of the impinging helium jets cause hot spots in the lower support plate and helium stratification in the LP. Results of sophisticated CFD calculations using SNL's Fuego code showed that using swirling inserts at the exit of the helium coolant channels in the VHTR core during operation effectively eliminates the formation of hot spots in the lower support plate and enhances the helium gas mixing in the LP region.

The Fuego simulations of the flow field in the LP of the VHTR used the dynamic Smagorinsky LES turbulence model, PMR, and CHT. The conventional helium jets were replaced with swirling jets with various swirl angles ranging from 30 to 75°. The calculations showed that significant enhancements in heat transfer, mixing, and entrainment can be achieved with the swirling jets.

REFERENCES

Arzutug, M. and S. Yapici, "Electrochemical Mass Transfer in Impinging Swirl Jets", *Ind. Eng. Chem. Res.*, **Vol.** 48, 1593-1602, 2009.

Blevins, R., *Applied Fluid Dynamics Handbook*, Krieger Publishing Company, Malabar, Florida, 1992.

Bilen, K., Bakirci, K., Yapici, S., and Yavuz, T., "Heat Transfer from a Plate Impinging Swirl Jet," *Int. J. Energy Res.*, **Vol.** 26, 305 – 320, 2002.

Bird, R., W. Stewart, and E. Lightfoot, "Transport Phenomena", John Wiley & Sons, 2nd Edition (2007).

Burns, S. P, "Applications of P Spatial and Angular Domain Based Parallelism to a Discrete Ordinates Formulation with Unstructured Spatial Discretization", Proceedings of the Second International Symposium on Radiation Transfer, 173-193, 1997.

Chevray, R. and N. K. Tutu, "Intermittency and Preferential Transport of Heat in a Round Jet", *J. Fluid Mech.*, **Vol.** 88, Part 1, 133-160, 1978.

Chigier, N. A. and Chervinsky, A., "Experimental Investigation of Swirling Vortex Motion in Jets", *ASME J. Applied Mechanics*, Series E, **Vol.** 3, 443-451, 1967.

CUBIT, http://www.cs.sandia.gov/capabilities/CubitMeshingProgram/index.html (2009).

Denev, J. A., J. Frohlich, and H. Bockhorn, "Large Eddy Simulation of a Swirling Transverse Jet into a Crossflow with Investigation of Scalar Transport", *Physics of Fluids*, **Vol.** 21, 2009.

Domino, S. P. *et al*., "Verification for Multi-Mechanics Applications, presented at the 48th AIAA/ASME/AHS/ASC Structures, Structural Dynamics, and Materials Conference, Honolulu, HI, 2007.

Germano, M. *et al*., "A Dynamic Subgrid-Scale Eddy Viscosity Model", *Physics of Fluids A*, Vol. 3, No. 7, 1760–1765, 1991.

Guililen, D. P. and H. M. McIlroy, "Preliminary Study of Turbulent Flow in the Lower Plenum of a Gas-Cooled Reactor", Proc. NURETH-12, Pittsburg, PA (2007).

INL, "Next Generation Nuclear Plant Pre-Conceptual Design Report", INL/EXT-07-12967, Rev. 1., Idaho National Laboratory (2007).

Johnson, R. W., "CFD Investigation of Experimental Data Proposed to be a Validation Data Set", INL/CON-09-15331, Proceedings of the 17th International Conference on Nuclear Engineering, July 12-16, ICONE 17-75604, Brussels, Belgium (2009a).

Johnson, R. W., "Examination of a Proposed Validation Data Set Using CFD Calculations", Proceedings of FEDSM2009, ASME 2009 Fluids Engineering Summer Meeting, August 2 – 5, Vail, Colorado (2009b).

Johnson, R. W. and R. R. Schultz, "Computational Fluid Dynamic Analysis of the VHTR Lower Plenum Standard Problem", INL/EXT-09-16325, Idaho National Laboratory (2009).

Kamotani, Y. and I. Greber, "Experiments on Confined Turbulent Jets in Cross Flow", NASA CR-2392, March 1974.

Kavsaoglu, M. S. and J. A. Schetz, "Effects of Swirl and High Turbulence on a Jet in a Crossflow", *J. Aircraft*, **Vol.** 26, No. 6, June 1989.

Kerr, N. M. and D. Fraser, "Swirl. Part I: Effect on Axisymmetrical Turbulent Jets". *J. of the Institute of Fuel*, **Vol.** 39**,** 519 – 526, 1965.

Lim, T. T., T. H. New, and S. C. Luo, "On the Development of Large-Scale Structures of a Jet Normal to a Cross Flow", *Physics of Fluids*, **Vol.** 13, No. 3, March 2001.

MacDonald, P. E. *et al*., "NGNP Preliminary Point Design – Results of the Initial Neutronics and Thermal-Hydraulic Assessments", Idaho National Laboratory, INEEL/EXT-03-00870 Rev. 1 (2003).

MacDonald, P. E., "Next Generation Nuclear Plant (NGNP) A Very High Temperature Gas-Cooled Reactor (VHTR)", Advanced Reactor, Fuel Cycle, and Energy Products, Workshop for Universities, March 4 – 5, Gaithersburg, MD (2004).

Mathur, M. L. and N. R. L. MacCallum, "Swirling Air Jets Issuing from Vane Swirlers. Part 1: Free Jets", *Journal of the Institute of Fuel*, **Vol.** 40, 214-225, 1967.

McIlroy, H. M., D. M. McEligot, and R. J. Pink, "Measurement of Flow Phenomena in a Lower Plenum Model of a Prismatic Gas-Cooled Reactor", Proceedings of the 16th International Conference on Nuclear Engineering (ICONE-16), May 11 – 15, Orlando (2008).

Moin, P. K. *et al*., "A Dynamic Subgrid-Scale Model for Compressible Turbulence and Scalar Transport", *Phys. Fluids A*, **Vol.** 3, No. 11, 2746–2757, 1991.

Pratte, D. and Baines, W. D., "Profiles of the Round Turbulent Jet in a Cross Flow", J. of the Hydraulics Division, Proceedings of the American Society of Civil Engineers, November, 1967.

PRO/ENGINEER, http://www.ptc.com/products/proengineer (2009).

Reichardt, H., Gesetzmassigkeiten der freien Turbulenz, VDI-Forschungsheft 414, 1942.

Ribner, H. S. and B. Etkin, "Noise Research in Canada", *Proc. 1st Int. Cong. Aero. Sci*., Madrid, 1958. (Also published by Pergamon Press, London, 1959.)

Rodriguez, S. B. and M. S. El-Genk, "Numerical investigation of potential elimination of 'hot streaking' and stratification in the VHTR lower plenum using helicoid inserts", *Nuclear Engineering and Design Journal*, **Vol.** 240, 995-1004 (2010a).

Rodriguez, S. B. and M. S. El-Genk, "Cooling of an Isothermal Plate Using a Triangular Array of Swirling Air Jets", 14th *International Heat Transfer Conference*, Washington DC, 2010b. (Draft submitted for review).

Rodriguez, S. B. and M. S. El-Genk, "On Enhancing VHTR Lower Plenum Heat Transfer and Mixing via Swirling Jets", *Proceedings of ICAPP '10*, Paper 10160, San Diego, CA, 2010c.

Schlichting, H., Boundary Layer Theory, McGraw-Hill Book Company, 7th Edition, New York, 1979.

Schultz, R. R., "Next Generation Nuclear Plant—Design Methods Development and Validation Research and Development Program Plan", INEEL/EXT-04-02293, Idaho National Engineering and Environmental Laboratory (2004).

Southworth, F. H. *et al*., "Next Generation Nuclear Plant (NGNP) Project – Preliminary Assessment of Two Possible Designs", 14th Pacific Basin Nuclear Conference, March 21 – 25, INEEL/CON-03-01014, Paper 91915 (2004).

Tutar, M. and A. E. Holdo, "Computational Modeling of Flow Around a Circular Cylinder in Sub-Critical Flow Regime with Various Turbulence Models", *Int. J. for Numerical Methods in Fluids*, **Vol.** 35, 763-784, 2001.

White, F., "Viscous Fluid Flow", 2nd Edition, McGraw-Hill, Inc., 1991.

Wikipedia, "Karman Vortex Street", http://en.wikipedia.org/wiki/K%C3%A1rm%C3%A1n_vortex_street. Accessed on February 2010.

Wilcox, D. C. Turbulence Modeling for CFD, DCW Industries, 2nd edition, 1998.

Williamson, C. H. K., "Oblique and Parallel Modes of Vortex Shedding in the Wake of a Circular Cylinder at low Reynolds Numbers", *J. Fluid Mech.*, **Vol.** 206, 579 – 627, 1989.